The journal is supported by the
Ukrainian School of Mining Engineering

Mining
of Mineral Deposits

Scopus

ELSEVIER

INDEXED IN EMERGING SOURCES CITATION (Web of Science) CLARIVATE ANALYTICS

Clarivate Analytics

QUARTERLY

Volume 19
Issue 4

ISSN 2415-3443 (Online)
ISSN 2415-3435 (Print)

JOURNAL HOMEPAGE
mining.in.ua
https://doi.org/10.33271/mining

Dnipro University of Technology
2025

The journal is supported by the
Ukrainian School of Mining Engineering

Mining
of Mineral Deposits

QUARTERLY

Volume 19
Issue 4

ISSN 2415-3443 (Online)
ISSN 2415-3435 (Print)

JOURNAL HOMEPAGE
mining.in.ua
https://doi.org/10.33271/mining

Dnipro University of Technology
2025

Журнал виходить за підтримки
Української школи гірничої інженерії

Розробка Родовищ

КВАРТАЛЬНИК

Випуск 19
Номер 4

ISSN 2415-3443 (Онлайн)
ISSN 2415-3435 (Друк)

ДОМАШНЯ СТОРІНКА
mining.in.ua
https://doi.org/10.33271/mining

Національний технічний університет
“Дніпровська політехніка”
2025

DNIPRO UNIVERSITY of TECHNOLOGY 1899

Dnipro University of Technology
19 Dmytra Yavornytskoho Ave., building 4, room 57,
49005, Dnipro, Ukraine
Certificate of Publisher DK No.1842
dated June 11, 2004

MMD JOURNAL / MINING.IN.UA

EDITORIAL OFFICE

EDITOR-IN-CHIEF	*Volodymyr Bondarenko*
DEPUTY EDITOR-IN-CHIEF	*Iryna Kovalevska*
DEPUTY EDITOR-IN-CHIEF	*Vasyl Lozynskyi*
MANAGING EDITOR	*Kateryna Sai*
ENGLISH LANGUAGE EDITOR	*Tetiana Vvedenska*

The journal is supported by the
Ukrainian School of Mining Engineering

Printed by LLC “LPres”
Coated paper, digital printing type
Passed for printing under the recommendation
of the Editorial Office of the journal
“Mining of Mineral Deposits”
(transaction No.1 dated December 30, 2025)
Number of copies printed 30
Sheet size 60×90/8

CONTENT

Q.P. Le, T.T. Vu
Numerical modeling analysis of floor stress distribution under coal pillars and roadway stability in close-distance coal seams 1 – 11

F. Kutllovci, B. Sinani
Geochemical distribution and correlations of Cd-Ag-Sb in relation to Pb-Zn mineralization at the Trepça mine, Kosovo 12 – 21

V. Morkun, N. Morkun, T. Oliinyk, S. Hryshchenko
Using a combined electromagnetic conversion method to determine iron ore characteristics 22 – 30

Yu. Vynnykov , S. Manhura, A. Aniskin, M. Rybalko, Yu. Nikolaienko, A. Manhura
Modeling corrosion crack resistance of oil tanks using neural network analysis 31 – 39

D. Brovko, R. Makareiko, S. Sakhno, L. Yanova, O. Pischikova
Numerical study of the influence of the angle of inclination and resistance of the mine workings on the formation of air flows during a fire 40 – 52

M. Munzareen, F. Bibi, S. Ihsan, K.S. Shah, M.Z. Emad
Advanced CNN-based remote sensing for mineral mapping of porphyry systems in the Gilgit region 53 – 62

S. Saptono, V. Vergiagara, R.F. Surachman, B. Dwinagara, O.W. Lusantono, A. Ardian, S.R. Haq
Field-based assessment of blast-induced vibration and slope stability in an andesite quarry 63 – 71

Z. Shen, M. Yan, D. Zhao
Machine learning model for windage alteration fault diagnosis of mine ventilation system under unbalanced samples 72 – 80

D. Miroshnichenko, M. Chemerinskiy, H. Bilushchak, S. Pyshyev, Yu. Rohovyi, O. Bogoyavlenska
Forecasting the characteristics of crude oil from the Druzhelyubivske oil and gas condensate field 81 – 90

T.D. Tung, L.C. Tuan, D.Q. Binh, H.S. Trinh, N.T. Quang
The characteristics of lead-zinc metallization in the Ban Kep area, Bac Me District, Ha Giang Province 91 – 98

R. Mussin, P. Małkowski, F. Murtazina, A. Kainazarova, D. Akhmatnurov, N. Zamaliyev, D. Doni
Integrated geophysical assessment of coal mass structural weakening zones for optimization of drilling-blasting operations and coal size control 99 – 118

O. Sinchuk, O. Mykhailenko, I. Sinchuk, M. Kotiakova, V. Baranovskyi, M. Baranovska
Adaptive control of power receivers supply voltage in underground mines 119 – 129

D.C. Birawidha, M. Amin, A. Miswanto, F.H. Jaya, S.U. Dewi, M.K. Nariswari, D.M. Putri
Variations in alumina-based material composition and heating temperature of refractory bricks in mullite formation 130 – 138

E. Lecaj, T. Serafimovski, M. Paçarizi
Risk assessment of potentially toxic elements in soil surrounding the Golesh ferronickel mine, Kosovo 139 – 146

S. Landar, A. Velychkovych, V. Vytvytskyi, L. Ropyak
Threshold vibration metrics of drilling tools as indicators of bit wear and rate of penetration decline: Field trials and data interpretation 147 – 157

ЗМІСТ

К.Ф. Ле, Т.Т. Ву
Чисельне моделювання розподілу напружень в підошві під вугільними ціликами та стійкість виробок у близькорозташованих вугільних пластах 1 – 11

Ф. Кутловці, Б. Сінані
Геохімічний розподіл і кореляції Cd-Ag-Sb щодо Pb-Zn мінералізації в родовищі Трепча, Косово 12 – 21

В. Моркун, Н. Моркун, Т. Олійник, С. Грищенко
Використання вихрострумового перетворення для реалізації комбінованого електромагнітного методу визначення характеристик залізної руди 22 – 30

Ю. Винников, С. Мангура, А. Аніскін, М. Рибалко, Ю. Ніколаєнко, А. Мангура
Моделювання корозійної тріщиностійкості нафтових резервуарів за допомогою нейромережевого аналізу 31 – 39

Д. Бровко, Р. Макарейко, С. Сахно, Л. Янова, О. Пищикова
Чисельне дослідження впливу кута нахилу та опору гірничих виробок на формування повітряних потоків під час пожежі 40 – 52

М. Мунзарін, Ф. Бібі, С. Іхсан, К.С. Шах, М.З. Емад
Передові технології дистанційного зондування на основі CNN для створення карт мінеральних ресурсів порфірових систем у регіоні Гілгіт 53 – 62

С. Саптоно, В. Вергіагара, Р.Ф. Сурахман, Б. Двінагара, О.В. Лусантоно, А. Ардіан, Ш.Р. Хак
Польова оцінка вибухових вібрацій і стійкості укосів в андезитовому кар'єрі 63 – 71

З. Шен, М. Ян, Д. Зао
Модель машинного навчання для діагностики відхилень опору у вентиляційній системі шахти за умов незбалансованих даних 72 – 80

Д. Мірошниченко, М. Чемеринський, Г. Білущак, С. Пиш'єв, Ю. Роговий, О. Богоявленська
Прогнозування характеристик нафти Дружелюбівського нафтогазоконденсатного родовища 81 – 90

Т.Д. Тунг, Л.К. Туан, Д.К. Бінь, Х.С. Трін, Н.Т. Куанг
Характеристика свинцево-цинкового оруднення в районі Бан Кеп, повіт Бак Ме, провінція Хазянг 91 – 98

Р. Мусін, П. Малковскі, Ф. Муртазіна, А. Кайназарова, Д. Ахматнуров, Н. Замалієв, Д. Доні
Інтегрована геофізична оцінка зон структурного ослаблення вугільного масиву для оптимізації буровибухових робіт та управління крупністю вугілля 99 – 118

О. Сінчук, О. Михайленко, І. Сінчук, М. Котякова, В. Барановський, М. Барановська
Адаптивне керування напругою живлення електроприймачів підземних рудників 119 – 129

Д.Ч. Біравідха, М. Амін, А. Місванто, Ф.Х. Джая, С.У. Деві, М.К. Нарісварі, Д.М. Путрі
Вплив складу алюмооксидних матеріалів та температури випалу вогнетривкої цегли на формування муліту 130 – 138

Е. Лечай, Т. Серафімовскі, М. Пачарізі
Оцінка ризику потенційно токсичних елементів у ґрунті навколо феронікелевого рудника Голеш, Косово 139 – 146

С. Ландар, А. Величкович, В. Витвицький, Л. Роп'як
Порогові метрики вібрацій бурильного інструмента як індикатори зносу доліт і зниження швидкості проходки: польові випробування та інтерпретація даних 147 – 157

Mining of Mineral Deposits
Volume 19 (2025), Issue 4, 1-11

https://doi.org/10.33271/mining19.04.001

Numerical modeling analysis of floor stress distribution under coal pillars and roadway stability in close-distance coal seams

Quang Phuc Le [1,2], Trung Tien Vu [1,2*]

[1] *Hanoi University of Mining and Geology, Hanoi, Vietnam*
[2] *Research Group: Sustainable Development of Mining Science, Technology and Environment, Hanoi University of Mining and Geology, Hanoi, Vietnam*

**Corresponding author: e-mail vutrungtien@humg.edu.vn*

Abstract

Purpose. The stability of the lower coal seam roadway under the condition of close coal seams is a key issue in underground mining, mainly when the roadway is located under the coal pillar of the upper seam. This paper analyzes the stress distribution rule under the coal pillar to determine the reasonable location of the roadway in the lower seam at Thong Nhat Coal Mine, Vietnam.

Methods. Numerical simulation model using FLAC3D software was conducted to investigate the distribution and redistribution of stress under the coal pillar and the goaf area, considering vertical-horizontal stress, physical parameters of rock and actual boundary conditions.

Findings. Four different roadway layout locations were assumed for comparison: Under the center of the pillar (A), under the edge of the pillar (B, C) and in the floor area under the goaf (D). The results showed that the highest stress concentration was at location A, with a concentration coefficient of 2.4-2.7 times the initial stress, creating a high risk of instability. Locations B and C had lower stresses but were still strongly affected by the pillar load. In contrast, location D showed a significantly lower and uniform stress distribution, and a small plastic zone development range, which was favorable for maintaining roadway stability.

Originality. The choice of roadway location is decisive for the safety and longevity of the project. In the geological conditions at Thong Nhat Coal Mine, arranging the roadway in the floor area under the goaf outside the coal pillar with a horizontal distance of 5m (location D) is the most reasonable and safest. At the same time, it is necessary to avoid arranging the roadway directly under the coal pillar.

Practical implications. The research results provide a scientific and practical basis for design work, improving stability, reducing maintenance costs and ensuring safety in underground mines with close coal seams.

Keywords: *coal pillar, coal seams, floor stress distribution, mining-induced pressure, roadway stability, Thong Nhat Coal Mine*

1. Introduction

Underground coal mining in Vietnam accounts for 95% of the total annual mining output of the coal industry. The complexity of underground coal mining always poses many risks to labor safety and production efficiency. In Vietnam, underground coal mining is carried out in the order of the upper coal seam first, then the lower coal seam. Early exploitation of the upper coal seams will break the connection of the rock layers and increase their displacement when exploiting the lower coal seam. In particular, when mining coal in areas with close coal seams, the pillars left in the upper coal seam lead to stress concentration in the floor, causing problems for mining operations and roadway protection in the lower coal seam [1], [2]. In fact, it is complicated to determine the characteristics of stress transmission and concentration in such complex mining conditions.

The pressure distribution on the coal pillar is affected by the load of the rock masses above within a specific range and is related to its width and properties [3]. Accordingly, the floor stress distributed by a coal pillar is very complicated. Wang et al. [4] analyzed that, when there is a coal pillar in the goaf, the stress distribution characteristics will follow the structure of "goaf-coal pillar-goaf". Under the coal pillar, the stress concentration can be 10 times that under the goaf. In areas of high stress, the rock mass is more likely to be in a plastic deformation state and will not be suitable for arranging the roadways.

Several hypotheses on the distribution of floor stress under coal pillars have been studied theoretically and in the laboratory by many scientists. The factors affecting the intensity and distribution of vertical pressure under coal pillars have been generally analyzed. In recent years, numerical techniques have been more strongly developed and more widely applied in underground coal mining research. To clarify the distribution of floor stress, some scholars [5]-[11] have established numerical models of close coal seams based on FLAC3D or UDEC software and studied the changes and characteristics of floor stress after mining the upper coal seam. Other scholars [12]-[16] first built mechanical models to analyze the distribution rule of floor stress qualitatively. Then they used numerical simulations to describe the distribution of floor stress and obtain quantitative data. Du et al. [17] analyzed the stress

Received: 16 May 2025. Accepted: 22 October 2025. Available online: 30 December 2025

© 2025. Q.P. Le, T.T. Vu

Mining of Mineral Deposits. ISSN 2415-3443 (Online) | ISSN 2415-3435 (Print)

This is an Open Access article distributed under the terms of the Creative Commons Attribution License (http://creativecommons.org/licenses/by/4.0/), which permits unrestricted reuse, distribution, and reproduction in any medium, provided the original work is properly cited.

distribution model while mining multiple coal seams at the Longde Coal Mine in western China.

With the help of numerical simulation, the 4 and 7 m wide destruction zones on both sides of the coal pillar were formed during the mining of adjacent longwalls. Finally, the authors calculated a 12.5 m wide coal pillar to ensure they were destroyed within the mining area. Jiang et al. [18] studied the influence of mining technological parameters on the deformation and stability of coal pillars during short longwall mining in ultra-thick coal seams and 1.0 km deep in eastern China. In this study, they found that the vertical stress under the floor of the coal pillar was proportional to the width of the goaf zone on both sides. Jun et al. [19] studied the stress change caused by mining when the longwall passed under the coal pillar at a close distance. They found that the bearing pressure increased rapidly as the longwall approached the coal pillar (reaching a maximum at a distance of 20 m) and then gradually decreased below the coal pillar. Liu et al. [20], as well as Vu et al. [21], [22], used UDEC software to study the stability of coal pillars when mining each layer close to each other based on the geological conditions of Gaohe Coal Mine, China and Nui Beo Coal Mine, Vietnam. Mu et al. [23] used the coal seam conditions in Xinzhouyao Mine, China, to study the destruction mechanism of the roadway during the mining of multiple seams under the upper coal pillar based on theoretical analysis and numerical simulation. Meanwhile, in Daliuta Coal Mine, Shanxi province, China, Piao et al. [24] studied the motion characteristics of mining the seam under the remaining coal pillar in the mining area based on the optical fiber monitoring method. Shan et al. [25] simulated the mining of close-distance coal seams to study the distribution characteristics of stress deviations in the surrounding rock mass in the lower coal seam.

Thus, previous studies have shown that the presence of coal pillars is the leading cause of the roadways' instability (including haulage level and ventilation level) in the close coal seam below. Compared with single-seam mining, a series of abnormal rock pressure phenomena, such as compression of the two sides of the roadway, floor push and deformation of the roadway, appear more seriously under the mining conditions of close seams. The stress concentration under the floor of the coal pillar is often several times higher than the normal state, which makes the roadway support and exploitation of the lower coal seam particularly difficult.

Although the negative impacts of coal pillars have been noted in many international studies, there has not been any research in Vietnam's underground coal mines that has delved into the stress mechanism and solutions to maintain the stability of the roadway. Therefore, this study will focus on analyzing the geological and mining conditions at Thong Nhat Coal Mine as a basis for building a numerical model, thereby analyzing and evaluating the stress distribution rule under the coal pillars and proposing the location of the roadway of the lower coal seam in the safe stress zone.

2. Methods

2.1. Study area

The study area was conducted at coal seams #6b and #6d of Thong Nhat Coal Mine. The 5-15 m thick siltstone is the rock layer between the two coal seams. The coal seam #6d is located above, with an average thickness of 2-4 m, an average slope angle of 3 degrees, and a depth of 300 m.

The length of the longwall is 120~140 m. The diagram of the panels and stratigraphic column in the study area is shown in Figure 1.

(a)

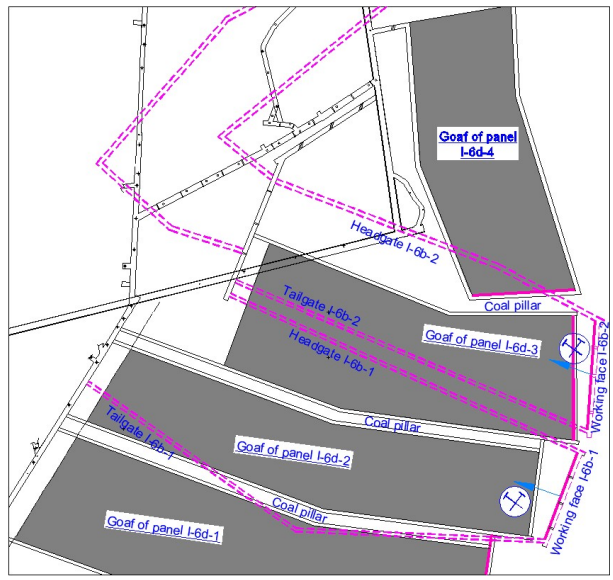

(b)

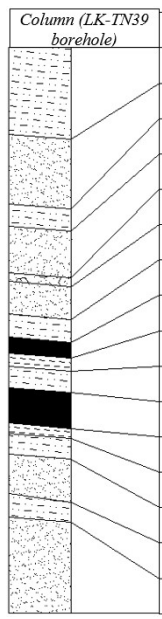

Column (LK-TN39 borehole)	Coal and rock strata	Thicksess (m)	Depth (m)
	mudstone	19.0	252.0
	sandstone	18.1	271.0
	mudstone	6.3	277.3
	sandstone	11.6	283.6
	fine-sandstone	2.0	295.2
	sandstone	8.2	297.2
	mudstone	5.8	305.4
	#6d coal seam	2.0-4.0	311.2
	siltstone	3.0	314.2
	mudstone	4.8	317.2
	#6b coal seam	6.0	322.0
	siltstone	2.5	324.5
	mudstone	4.5	329.0
	sandstone	9.5	338.5
	mudstone	5.0	343.5
	sandstone	30.0	373.5

Figure 1. The diagram of the panels (a) and stratigraphic column (b) in the study area of Thong Nhat Coal Mine

The 20-30 m wide coal pillar is usually left in the goaf. Currently, the coal seam #6d has almost been fully exploited. The lower coal seam #6b is being prepared and exploited at the first longwall. The average thickness of the coal seam #6b is 6 m, the average slope angle is 3 degrees, and the depth is 310 m. The stress concentration under the floor of the coal pillar significantly affects the stress of the primary rock mass and the stability of the Seam #6b roadway. Therefore, the roadway layout in the lower seam is of great importance for exploiting coal seam #6b. The physical properties of coal and rock mass in the study area are shown in Table 1.

Table 1. The physical properties of coal and rock mass in the study area of Thong Nhat Coal Mine [26]

Type rock	Fine-sandstone	Sand-stone	Mud-stone	Silt-stone	Coal
Tensile strength, MPa	1.75	1.63	0.98	1.25	0.5
Bulk modulus, GPa	8.12	7.451	2.342	1.826	0.755
Shear modulus, GPa	3.642	3.24	0.95	0.609	0.486
Poisson's ratio	0.3	0.31	0.32	0.34	0.26
Cohesion, MPa	3.15	3.21	2.16	1.83	1.45
Friction angle, deg.	38	34	30	26	25
Density, kg/m^3	2840	2775	2556	2250	1460

2.2. Analysis of stress formation below the coal pillar

Currently, measuring stresses at the location under coal pillars or in the goaf is impossible. Therefore, they are often estimated through the load on the coal pillar from the covering layers. There are three different types of pressure charts distributed along the width of the coal pillar, commonly found in underground coal mines, namely: two-peak stress form (in wide coal pillars), has the form of a prominent stress peak (in medium-wide coal pillars), and has the form of a small stress peak (in narrow coal pillars). The concentrated stress that appears due to the loading of rock masses on the pillar will be transmitted downward, causing stress redistribution in the floor. Within a specific range inside the coal pillar, the bearing capacity and the impact pressure will reach a state of limit equilibrium. The limit equilibrium theory has been used in previous studies to determine the width of the plastic stress zone in the coal pillar [27]-[30]. Based on these studies, a plastic stress zone X_0 will form at the edge of the coal pillar, determined by the following Formula:

$$X_0 = \frac{m}{2\zeta f}\ln\frac{k\gamma H + \dfrac{C}{\tan\varphi}}{\zeta\left(p_1 + \dfrac{C}{\tan\varphi}\right)}, \qquad (1)$$

where:

m – the height of the coal pillar (corresponding to the mining height of the coal seam), m;

$\zeta = \dfrac{1+\sin\varphi}{1-\sin\varphi}$ – represented by the triaxial stress coefficient;

$f = \dfrac{\tan\varphi}{4}$ – the friction coefficient between the coal seam and the rock;

k – the stress concentration coefficient;

γ – the average volumetric force of the upper layers, kN/m^3;

H – the calculated depth of the structure, m;

C – the coal cohesion force, kN/m^3;

φ – the internal friction angle of the coal, degree;

p_1 – the hydraulic support resistance at the edge of the coal pillar, MPa.

The practice at Thong Nhat Coal Mine shows that the hydraulic support resistance at the edge of the coal pillar has no noticeable effect on the extent of the limited equilibrium zone; therefore, $p_1 = 0$. The stress concentration coefficient found in underground coal mines in Vietnam is $k = 2.5$-2.7, averaging 2.6 [31]. With the base of the coal seam #6d, according to Formula (1), the width of the plastic stress zone at the edge of the coal pillar is determined as shown in Table 2.

The calculation results show that the width of the plastic zone also increases proportionally with the coal seam's thickness and the mine's depth.

Table 2. Width of plastic stress zone at coal pillar edge of coal seam #6d

X_0, m	m, m	ζ	f	k	γ, kN/m^3	H, m	C, kN/m^3	ϕ, deg	p_1, MPa
3.8	2	2.464	0.117	2.6	25	300	1450	25	0
4.2	2	2.464	0.117	2.6	25	350	1450	25	0
4.6	2	2.464	0.117	2.6	25	400	1450	25	0
7.5	4	2.464	0.117	2.6	25	300	1450	25	0
8.5	4	2.464	0.117	2.6	25	350	1450	25	0
9.3	4	2.464	0.117	2.6	25	400	1450	25	0

At the depth limit of 300 m of seam #6d, the plastic deformation zone's width at the coal pillar's edge is determined as $X_0 = 3.8$ m and 7.5 m, corresponding to the coal seam thickness of 2 m and 4 m, respectively. In the case where tectonic stress is excluded, the floor stress model under the coal pillar is shown in Figure 2.

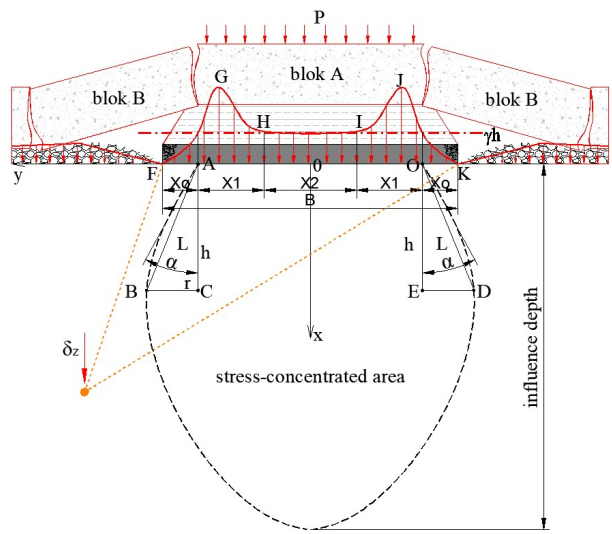

Figure 2. Characteristic diagram of stress distribution in the presence of coal pillars

The diagram in Figure 2 shows that the AF and OK sections are the plastic zone ranges on both sides of the coal pillar. The GH and IJ sections are the elastic zone ranges, respectively, and the HI section is the initial rock stress range, with the value of γH. The characteristics of the rock collapse rule in the presence of a coal pillar are as follows:

– the immediate roof collapses into the goaf;

– the main roof bends, sinks, then rotates, breaks, and finally touches the rock in the goaf, and is then compressed.

Also in Figure 2, the load p_i on the coal pillar can be expressed as follows:

$$\begin{cases} p_1 = \dfrac{k\gamma H}{X_0}\left(z + \dfrac{B}{2}\right); & -\dfrac{B}{2} \le z \le -\left(\dfrac{B}{2} - X_0\right) \\ p_2 = \dfrac{\gamma H}{X_1}\left[(k-1)\left(z + \dfrac{X_2}{2}\right) - X_1\right]; & -\left(X_1 + \dfrac{X_2}{2}\right) \le z \le -\dfrac{X_2}{2} \\ p_3 = \gamma H; & -\dfrac{X_2}{2} \le z \le \dfrac{X_2}{2} \end{cases}, \qquad (2)$$

where:

X_0 – the plastic zone on both sides of the coal pillar, m;

X_1 – the elastic zone in the coal pillar, m;

X_2 – the initial stress zone, m;

B – the width of the coal pillar, m;

k – the stress concentration coefficient;

γ – the average volumetric force of the upper layers, kN/m^3;

H – the depth of the mine structure, m.

Analysis of stress concentration and reduction on the coal pillar shows that there will be a plastic zone at the two edges of the coal pillar (Fig. 2). In this zone, the coal cracks and releases stress. Furthermore, the main roof bends, sinks and transfers most of the load into the goaf zone. Therefore, there is no effect of transferring stress to the floor at the two edges of the coal pillar. The stress transmission range is mainly in sections $2X1 + X2$.

For the segment of $2X1 + X2$, considered as a semi-infinite flat object, the vertical stress propagation at any point with coordinates (x, y) below the coal pillar can be determined by the following Formula:

$$\delta_z = \frac{p}{\pi}\left[\begin{array}{c}\arctan\dfrac{y-\dfrac{2X_1+X_2}{2}}{x} - \arctan\dfrac{y+-\dfrac{2X_1+X_2}{2}}{x} + \\ \dfrac{x\left(y-\dfrac{2X_1+X_2}{2}\right)}{x^2+\left(y-\dfrac{2X_1+X_2}{2}\right)^2} - \dfrac{x\left(y+\dfrac{2X_1+X_2}{2}\right)}{x^2+\left(y+\dfrac{2X_1+X_2}{2}\right)^2}\end{array}\right], \quad (3)$$

According to Formula (3), the stress distribution curve under the floor of the coal pillar is described similarly to Figure 2. The stress concentration area has an elliptical shape with the axis passing through the center of the coal pillar. The stress distribution range in width and depth will be proportional to the width and position of the pillar under the rock layers. At a certain depth, the vertical stress near the center of the coal pillar will be the largest, and then gradually decrease to both sides [32]. Therefore, a narrow coal pillar will effectively reduce the spread of stress to the floor of the pillar. In this case, the coal pillar reaches a plastic state with many cracks. Stress release is achieved in this case; therefore, transmitting stress to the floor is unaffected. In this case, the roadway arrangement under the coal pillar is favorable. On the contrary, when wide coal pillars are left, the roadway arrangement under the coal pillar must be calculated to ensure that they are outside the area of high stress concentration.

In wide coal pillars, it is relatively possible to describe the stress under the pillar as being spread downwards in an ellipse (Fig. 2). The high stress zone will be entirely within the area of the ellipse (the central range of the coal pillar), and outside of it will be the primary stress zone. Thus, the roadway in the lower coal seam will be suitable for arrangement outside the ellipse area. In Figure 2, straight lines represent the AB (OD) arcs to simplify the calculation. Then, the deflection angle ∠BAC (∠DOE) will be characterized as the stress diffusion angle, and is determined by the following Formula:

$$\tan\alpha = \frac{r}{h}, \quad (4)$$

where:

r – the boundary point on the ellipse boundary and the limiting position of the plastic zone in the coal pillar, m;

h – the vertical distance between the calculation point and the coal pillar.

The stress diffusion angle can be easily determined in an elastic, homogeneous, and isotropic medium. However, with the characteristics of underground coal mines, determining this value becomes more difficult due to its dependence on the elastic modulus, strength and cohesion of the coal and rock layers. The results may affect the determination of the reasonable location of the roadway in the lower coal seam. A suitable support tool in the current stage is numerical simulation. In this paper, based on Thong Nhat Coal Mine, numerical simulation is used to clarify the stress propagation under the floor of the pillar and the roadway layout of the lower coal seam.

2.3. Numerical simulation analysis method

Numerical modeling is a modern method that can accurately investigate the stress distribution in rock mass and roadway stability during underground coal mining. Therefore, this is also the preferred method we use in this work. One of the popular programs for studying the stress environment in rock mechanics, the FLAC3D program [33], was chosen. The Flac3D program was chosen to be used in this study. This program uses the foundation of a finite element model with construction materials such as coal and stone, which are considered elastic materials that meet the Mohr-Coulomb durability criteria.

Coal seams #6d and #6b of Thong Nhat Coal Mine, Vietnam (Fig. 1) serve as the technical base providing input parameters for this study. The study aims to find the rule of concentrated stress transmission due to the remaining coal pillar at seam #6d to the floor and its influence on the roadway at seam #6b (lower seam). The study cases have thicknesses of seam #6d (upper seam) of 2 and 4 m, respectively. The width of the coal pillar is 20 and 30 m, respectively. The length of the longwall is 120 m. Between seams #6d and #6b, the claystone and siltstone layers have an average total thickness of 7.8 m. The main information about the rock and coal layers was shown in Figure 1 and Table 1.

Spatially, the model is set to have a length of 350 m in the X direction, a width of 265 m in the Y direction and a height of 140 m in the Z direction. Horizontal displacement is fixed for the side boundary. Both horizontal and vertical displacement are fixed for the bottom boundary. The model does not limit the displacement at the top boundary. A vertical stress of 6.5 MPa is applied to the top boundary of the model to simulate natural loads. A value of 0.025 MN/m^3 is assigned to the rock strata's specific weight, and gravity is also applied. The model's geological and rock mechanics parameters are similar to the conditions of the Thong Nhat Coal Mine study area (Table 1). The model structure diagram is presented in Figure 3.

To determine the appropriate location of the roadway in the lower coal seam (seam #6b), a rectangular roadway was designed with a width of 4m and a height of 3 m. In the presence of a coal pillar, the stability of the roadway in the lower coal seam was studied in the cases at locations A, B, C or D (Fig. 3).

3. Results and discussion

3.1. Stress distribution rule under the coal pillar of seam #6d

The results of stress distribution under the coal pillar of seam #6d are shown in Figure 4. The results from Figure 4 show that as the thickness of the coal seam increases, the stress concentration under the floor of the pillar decreases. The stress at a distance of 5 m below the pillar for a 2 m thick seam is 18.15 MPa, but this value is 14.38 MPa for a 4 m thick seam. At a distance of 15 m below the 30 m wide coal pillar (Fig. 4c), the stress value is 15.46 MPa for a 2 m thick seam, and this value is 9.72 MPa for a 4 m thick seam (Fig. 4d).

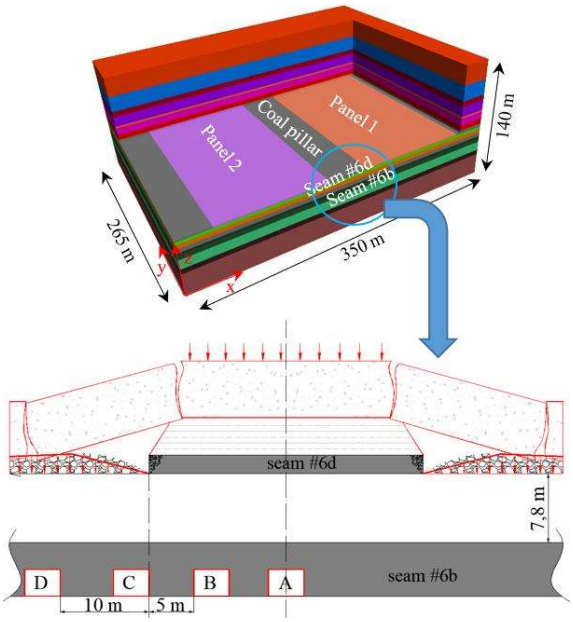

Figure 3. Structure of the research model and determination of the tunnel location of the lower seam

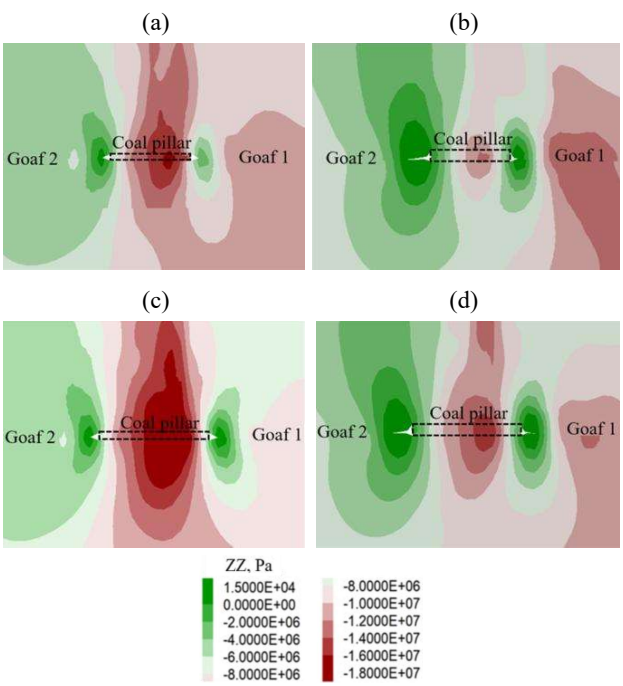

Figure 4. Vertical stress distribution under the coal pillar of seam #6d: (a) 20 m wide pillar, 2 m thick seam; (b) 20 m wide pillar, 4 m thick seam; (c) 30 m wide pillar, 2 m thick seam; (d) 30 m wide pillar, 4 m thick seam

This can be explained by the fact that, as the coal seam's thickness increases, the coal pillar's height also increases. The impact of the load from the upper rock layer is the cause of the development of cracks on both sides of the coal pillar.

This phenomenon occurs more intensely when the pillar's height (or the coal seam's thickness) increases. This process is synonymous with breaking the coal bond on both sides of the pillar and makes them easily destroyed. When the coal pillar is destroyed, it is not the main load-bearing object of the rock wall, but the load is transferred to the collapsed rock block in the goaf. Therefore, the stress distribution under the coal pillar is minimal. On the contrary, when the coal seam is thinner or the height of the coal pillar is smaller, the cross-section of the coal pillar is small, so the possibility of them being broken is very low. Therefore, they can maintain stability better than coal pillars with a significant height. However, the more stable the coal pillar is, the higher the stress concentration under the floor. It can also be affirmed that the stress concentration under the floor of the coal pillar is inversely proportional to the pillar's height (or the coal seam's thickness).

The stress is distributed throughout the coal pillar from top to bottom in the shape of a flattened ellipse. The ellipse's center is located on the coal pillar and towards the first longwall mined (right). The thicker the coal seam, the more clearly the center of the stress concentration ellipse develops. In Figure 4, the ellipse's center is 10 m from the edge of the coal pillar on the first longwall, while it is 20 m from the edge of the coal pillar on the second longwall. This may be because during the period of being influenced by the bearing pressure from the first longwall mining process, the right side of the coal pillar was compressed with the roof control process in the mining area. The stress peak is not entirely concentrated on the coal pillar and spreads into the coal seam on the unexploited second longwall side. During the exploitation phase of the second longwall, the coal pillar will bear the load independently and be affected a second time by the bearing pressure from the longwall mining process. The coal pillar on the first longwall side (which has been compacted) will bear the load better than the one on the second longwall side. Therefore, the center of the stress concentration zone will be shifted towards the pillar with a more stable structure.

The elliptical stress concentration zone will develop broader and deeper below the floor as the coal pillar's width increases and the coal seam's thickness decreases. In contrast, a narrow coal pillar has almost no stress concentration zone below the floor of the pillar. This proves that a narrow coal pillar has been destroyed. In a wide coal pillar, the stress concentration zone forms from the center and develops widely. In particular, a broad and thin coal pillar (2 m) has a large stress concentration zone that develops deep below the floor of the pillar as observed during the simulation.

3.2. The rule of plastic deformation zone formation under the coal pillar of seam #6d

The results of stress distribution in the plastic deformation zone under the coal pillar of Seam #6d are shown in Figure 5.

Figure 5 shows that the plastic deformation zone under the coal pillar floor is not apparent when the thickness of the coal seam is changed. However, when the width of the coal pillar is changed, the variation of the plastic deformation zone has been observed. In a coal pillar with a small width (20 m), the possibility of forming a plastic deformation zone is limited to a depth of 19.5 m below the floor. In a coal pillar with a width of 30 m, the plastic deformation zone develops deeper than in the previous case (up to 20.3 m). Although the change in value is insignificant, it still reflects the development of the plastic deformation zone's size corresponding to the coal pillar's width.

The characteristics of the rock mass in the plastic deformation zone reflect the appearance of cracks, the displacement of the rock mass and the reduction of cohesion, even the fragmentation. Therefore, the arrangement of the roadway in this area will be seriously affected by the following reasons.

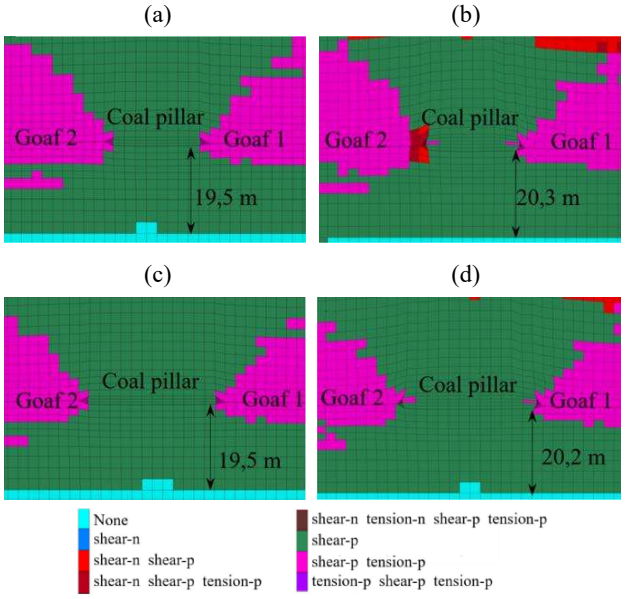

Figure 5. Stress distribution in the plastic deformation zone under the coal pillar of seam #6d: (a) 20 m wide pillar, 2 m thick seam; (b) 20 m wide pillar, 4 m thick seam; (c) -30 m wide pillar, 2 m thick seam; (d) 30 m wide pillar, 4 m thick seam

The rock mass moves into the roadway space and causes the supports to deform, losing their support ability. The roof is compressed on the support and the additional effect of cracking and loosening, causing the roof falling of the roadway. The rock mass on the floor is pushed by strong force, causing the floor push of roadway, narrowing the usable space of the roadway, and at the same time affecting transportation.

3.3. Choosing the correct location for the roadway in coal seam #6b

The above analysis shows that the roadway stability of the lower coal seam is governed by the stability of the coal pillar and the stress transmission model through it. Based on the stress distribution model and the extent of the plastic deformation zone analyzed, the hypothetical locations of the roadway were constructed, taking into account the specific geological-technical conditions in the study area. In the case of a 20 m or 30 m wide coal pillar retained in the exploited coal seam #6d area, the roadway is located 7.8 m below the coal pillar.

3.3.1. Stress distribution around the roadway under coal seam #6d

Under typical study conditions, coal seam #6b is located below the exploited area of coal seam #6d above. Corresponding to the layout locations of the roadway (Fig. 3), the results in Figure 6 and 7 show the stress distribution around the roadways when excavating them under coal pillars of 20 and 30 m wide, respectively.

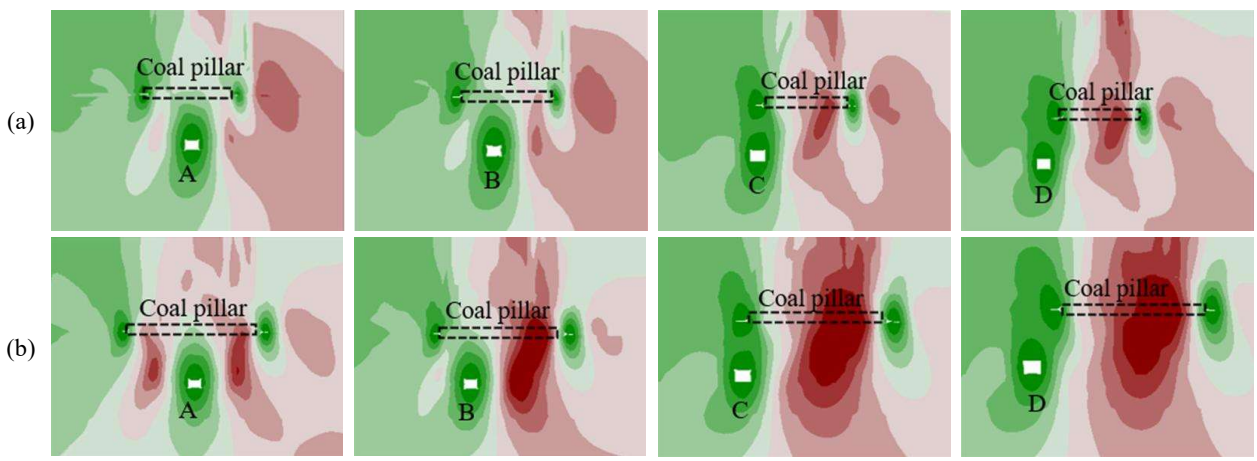

Figure 6. Stress distribution around the roadway under the 2 m thick coal seam #6d: (a) 20 m wide coal pillar; (b) 30 m wide coal pillar

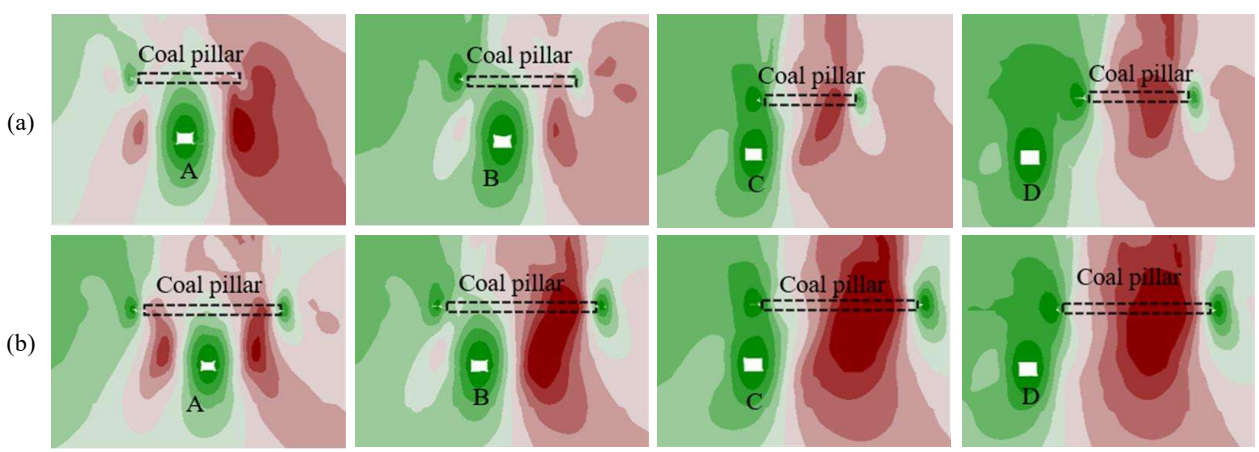

Figure 7. Stress distribution around the roadway under the 4m thick coal seam #6d: (a) 20 m wide coal pillar; (b) 30 m wide coal pillar

When considering the overall simulations in Figures 4, 6 and 7, the stress distribution rule is clearly and consistently shown: Before the roadway excavation, the vertical stress field is usually concentrated directly below the center of the pillar, creating a high stress core with a stress concentration factor of about 2.4-2.7 compared to the initial stress, while the two adjacent regions facing the goaf show reduced stress. Therefore, when a roadway is excavated directly below the center of the pillar (location A), this roadway not only bears a large vertical load from the pillar above but also changes the local stress redistribution process around the roadway. In other words, location A falls right at the "dangerous stress point", which can lead to the most significant risk of stress concentration and is the most unfavorable location regarding stress stability. The more off-center location (location B) is affected indirectly. There, the stress is reduced compared to that below the center of the coal pillar, but still has a significantly immense value due to the edge effect of the pillar (stress concentration coefficient of about 1.5-2.2 compared to the initial stress). Therefore, a roadway excavated at location B will cause moderate stress redistribution (not as severe as at location A) but requires roadway reinforcement because the stress value is still high. At the location near the edge of the coal pillar (location C), the stress field becomes more asymmetric. At the edge of the coal pillar, a strong gradient appears between the high stress zone (near the center) and the reduced zone (towards the goaf). Therefore, the roadway at location C will be affected by significant moments, causing the roadway and the rock mass to slide. Meanwhile, location D is near the stress reduction zone due to the load-bearing upper goaf (the concentration factor is only about 0.9-1.0 compared to the initial stress). The vertical stress is more favorable at this location than in the above cases. However, the long-term stability of the roadway will depend mainly on the settlement, shrinkage and collapse of the goaf.

Increasing the coal pillar's width and the coal seam's thickness will amplify the above effects. With a wider coal pillar and a thicker seam, the stress core under the pillar center will be deeper and of greater intensity. Therefore, any roadway closer to the pillar center will be substantially disadvantaged.

From the reality at Thong Nhat Coal Mine, the mandatory case when the roadway is located at position A is the pillar center which must lead to two practical consequences: first, the arrangement of the roadway right under the pillar center requires strong reinforcement measures and load-reducing measures (e.g. long anchors, load-bearing support, pressure-reducing drills); second, when there is a choice, priority should be given to the lower stress areas (positions B, C and D).

3.3.2. Distribution of plastic deformation zones around the roadway under the coal seam #6d

The results in Figure 8 and 9 show the distribution of plastic deformation zones around the roadway under coal seam #6d with thicknesses of 2 and 4 m respectively. The width of the coal pillar is 20 and 30 m, respectively.

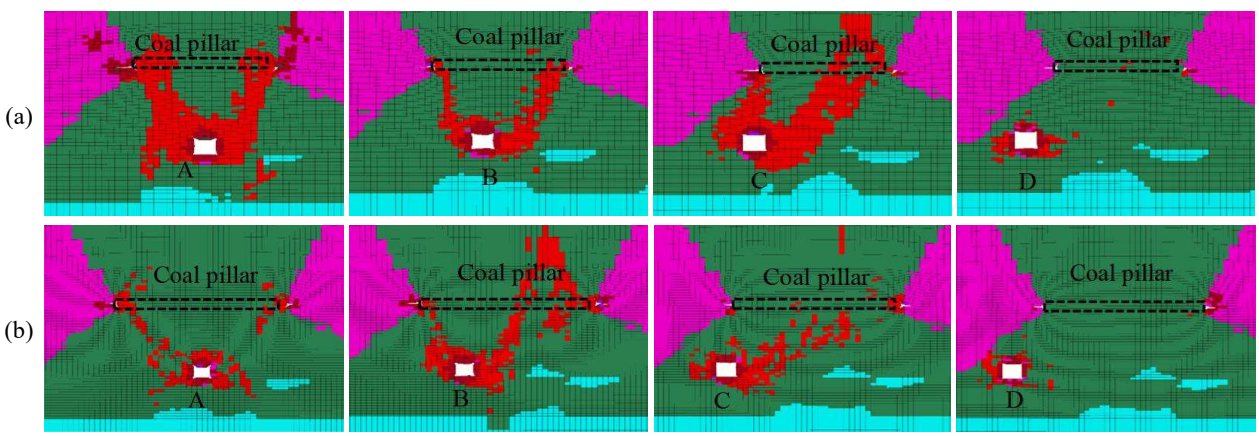

Figure 8. Distribution of plastic deformation zones around the roadway under the 2 m thick coal seam #6d: (a) 20 m wide coal pillar; (b) 30 m wide coal pillar

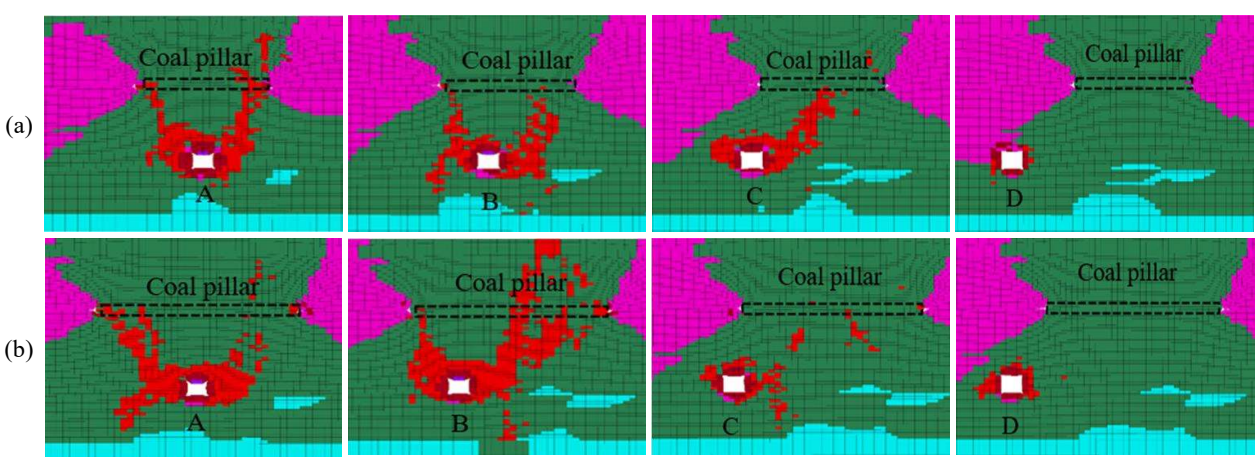

Figure 9. Distribution of plastic deformation zones around the roadway under the 4 m thick coal seam #6d: (a) 20 m wide coal pillar; (b) 30 m wide coal pillar

The simulation results of the development of the plastic deformation zone (Figs. 5, 8, and 9) show that the distribution rule is directly affected by the characteristics of the vertical stress field under the coal pillar and the location of the roadway. In the initial state (Fig. 5), the plastic deformation bands are concentrated on both sides of the pillar, where the stress gradient is large and the shear-tension condition is larger. In contrast, the area under the center of the pillar is still mainly elastic with high compressive stress. When the roadway is excavated at different locations, the morphology of the plastic deformation zone changes significantly, reflecting the local stress redistribution. Specifically, at position A (below the center of the coal pillar), the roadway is dug through the area of highest compressive stress, so the plastic deformation zone develops symmetrically around it with the boundary extending both at the wall and the pillar, showing the most unfavorable condition for stability. At position B, the deformation zone is mainly concentrated at the roof and the side near the edge of the pillar; the extent of spread is reduced compared to A, but still significant due to the boundary effect. Notably, at position C, where the roadway is dug close to the edge of the pillar, the plastic deformation zone develops asymmetrically, often extending towards the goaf, reflecting the state of compressive stress reduction transition stress, which increases the risk of local instability due to roof collapse or side sliding.

On the contrary, position D is near the stress reduction zone due to the upper goaf. This position shows that the development of the plastic deformation zone is relatively limited, mainly locally around the side and the floor of the roadway. This location has more favorable conditions for bearing capacity immediately after excavation, but long-term risks may arise due to secondary deformation from the goaf subsidence process.

Thus, the influence of pillar size and seam thickness is clearly shown: wide pillars and thick seams not only increase the intensity of stress concentration but also amplify the range of plastic deformation zone around the roadway, especially obvious at positions A and C. Thus, the general trend can be confirmed: the center of the pillar (A) and the edge of the pillar (C) are the most unfavorable positions in terms of plastic deformation development; the transition zone (B) has an intermediate level; while near the goaf (D) is the most favorable position, but it is necessary to monitor subsidence and landslide over time.

3.3.3. Evaluation of the convergence of roadways in different cases under coal seam #6d

The results in Figure 10 show the evaluation of the roadway convergence for the respective cases of seam thickness of 2 and 4 m, coal pillar width of 20 and 30 m. The results of stress and plastic deformation data analysis are reinforced by the convergence curve of the roadway at four locations, A, B, C and D. As summarized in Figure 10, the deformation of the roadway depends closely on the relative position under the coal pillar.

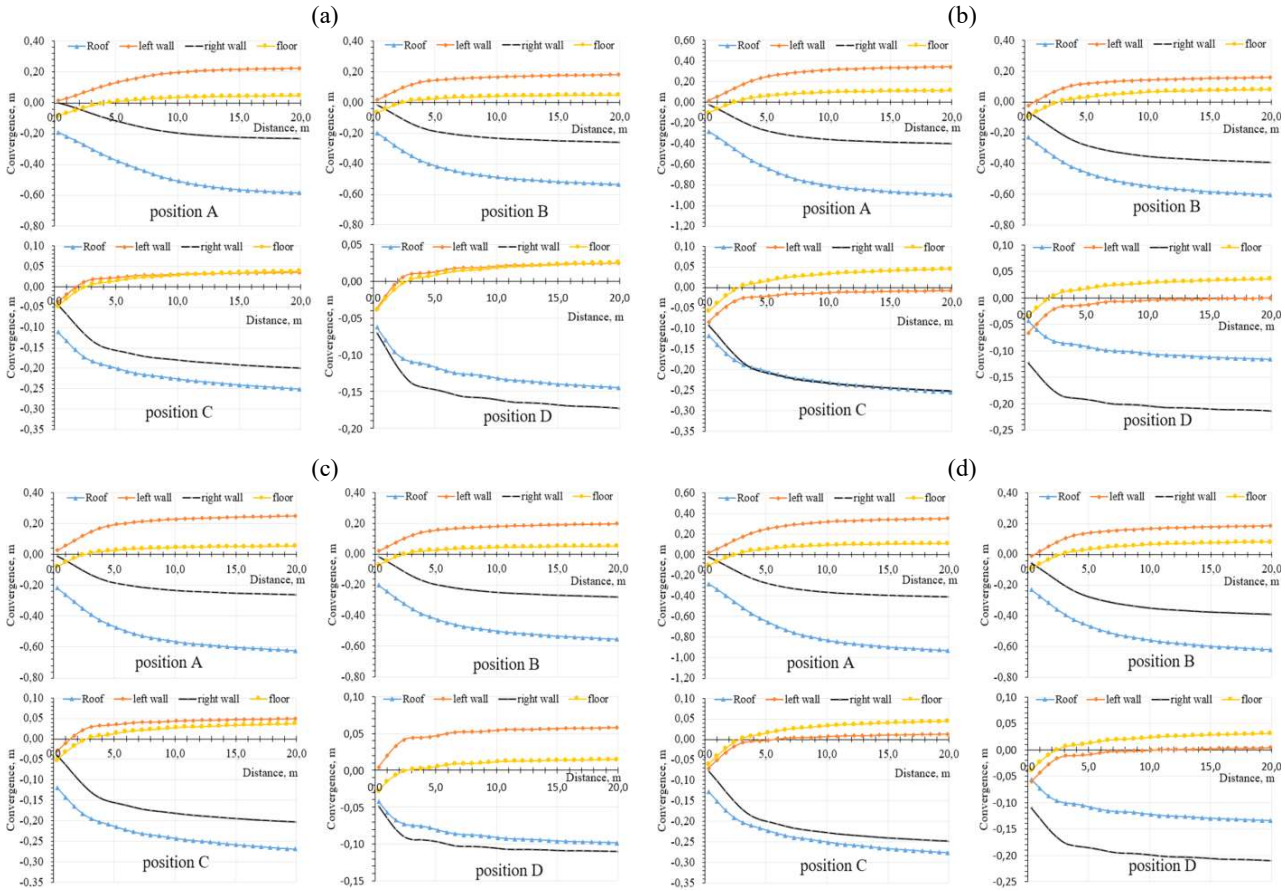

Figure 10. Evaluation of the convergence of the roadways in different cases: (a) 20 m wide coal pillar, 2 m thick seam; (b) 30 m wide coal pillar, 2 m thick seam; (c) 20 m wide coal pillar, 4 m thick seam; (d) 30 m wide coal pillar, 4 m thick seam

At location A, located directly under the center of the coal pillar, the convergence of the top reaches 0.6-0.95 m, and the convergence of the two sides reaches 0.2-0.4 m. The roadway's deformation law increases with the pillar's width and the seam's thickness. Thus, the vertical stress is most concentrated, leading to the symmetrical and extensive development of the plastic deformation zone around the roadway. The direct consequence is that the convergence amplitude here reaches the most significant value, and the rate of increase is rapid in the early stages after tunnel excavation. It tends to stabilize later than other locations. This confirms that arranging the roadway right under the center of the pillar is the most unfavorable option in terms of both stress and deformation.

At position B, due to the impact from the pillar edge, the stress field tends to be eccentric, and the plastic deformation zone develops strongly in the roof and side of the roadway (near the edge of the coal pillar). The roof convergence reaches 0.58-0.62 m, and the convergence on both sides is from 0.19-0.4 m. The asymmetry between the two sides is directly reflected in the convergence curve: the deformation amplitude is smaller than A but still maintains at a high level, and the convergence variation often has two distinct stages – initially fast due to local instability, then gradually slows down when the new support system is established.

For position C, close to the edge of the pillar and near the pressure reduction zone, the development of the plastic deformation zone is asymmetrical, mainly pulling towards the goaf. The convergence curve here shows strong oscillation characteristics. The deformation increases rapidly due to local cracking and side sliding, alternating with a deceleration phase when the stress is released towards the goaf. The roof convergence reaches 0.25-0.28 m, the left side convergence is about 0.04 m, and the correct side convergence is 0.2-0.25 m. Thus, although the convergence amplitude does not reach the maximum value at position A, the curve's complexity and unpredictability make position C have a high risk of instability.

On the contrary, position D is the position where the stress reduction effect from the goaf is dominant. Therefore, the plastic deformation zone is limited, locally concentrated around the side and the roadway floor. The corresponding convergence curve shows the smallest deformation value, slow growth rate and early steady state. The convergence of the roadway roof is 0.09-0.14 m, the left side is about 0.02-0.05 m, and the right side is 0.11-0.21 m. Therefore, this position has more favorable conditions for the roadway layout. However, it is still necessary to consider the secondary deformation due to the subsidence of the goaf over a long period.

The synthesis of the above analyses can conclude that the convergence transformation trend is entirely consistent with the stress distribution and plastic deformation zone: location A is the most unfavorable, followed by B and C, while D is the most feasible option to maintain the stability of the roadway. This emphasizes the importance of choosing a reasonable location for the roadway under the coal pillar, and at the same time provides clear guidance for the appropriate support solutions for each specific stress field condition.

4. Conclusion

The research results for typical conditions at Thong Nhat Coal Mine, Vietnam, allow the paper to draw several conclusions.

The strongest concentrated stress forms right under the center of the coal pillar, gradually decreasing to both sides and spreading down the roadways arranged under the lower seam. This is the fundamental cause leading to the apparent difference in the stability of the roadway between locations A, B, C and D.

The plastic deformation zone develops strongly under the center of the pillar (location A) and at the edge of the pillar (location C). The spread of this zone around the roadway can cause early destruction of the rock structure, creating conditions for intense roadway deformation. Meanwhile, at locations B and D, the plastic deformation range is narrower, creating favorable conditions for maintaining the stability of the roadway.

On a broader coal pillar and thicker seam, there will be a tendency to increase the size of the concentrated stress zone and the plastic deformation range, making the adverse impact on the lower roadway more obvious. This shows a nonlinear relationship between the geometry of the coal pillar and the stability of the roadway below it.

The research results also outline a complex picture when exploiting the close coal seams. In this mining condition, there is no "absolutely safe" position to arrange the roadway under the coal pillar. Therefore, the roadway location should be selected at a less risky location. With the paper's results, location D is the most reasonable, but it is still necessary to pay attention when combining suitable support and additional reinforcement solutions.

Author contributions

Conceptualization: QPL; Formal analysis: TTV; Methodology: QPL, TTV; Writing – original draft: QPL; Writing – review & editing: TTV. All authors have read and agreed to the published version of the manuscript.

Funding

This research is funded by the Vietnam Ministry of Education and Training (MOET) under grant number B2024-MDA-03.

Acknowledgements

Hereby, the authors express their gratitude to the Department of Engineering and Technology of the Thong Nhat Coal Mine staff for creating favorable conditions for data collection and field survey. At the same time, the authors also thank the Editors of the journal of Mining of Mineral Deposits for their comments to complete this paper.

Conflicts of interest

The authors declare no conflict of interest.

Data availability statement

The original contributions presented in the study are included in the paper, further inquiries can be directed to the corresponding author.

References

[1] Zhang, Y. (2020). Distribution law of floor stress during mining of the upper protective coal seam. *Science Progress*, *103*(3), 1-15. https://doi.org/10.1177/0036850420930982

[2] Wu, G., Fang, X., Bai, H., Liang, M., & Hu, X. (2018). Optimization of roadway layout in ultra-close coal seams: A case study. *PLOS ONE*, *13*(11), e0207447. https://doi.org/10.1371/journal.pone.0207447

[3] Zhang, G.-C., He, F.-L., Jia, H.-G., & Lai, Y.-H. (2017). Analysis of gateroad stability in relation to yield pillar size: A case study. *Rock Mechanics and Rock Engineering*, *50*(5), 1263-1278. https://doi.org/10.1007/s00603-017-1168-8

[4] Wang, N., Yang, D., Wang, Y., & Li, Y. (2024). Reasonable layout range of lower mining roadways in the close and variable interval coal seams mining: A case study. *Scientific Reports*, *14*(1), 23490. https://doi.org/10.1038/s41598-024-23490-4

[5] Zhang, H., Wang, L., Zhang, C., & Bai, Q. (2021). Study on stress distribution characteristics of floor roadway in close distance coal seams based on FLAC3D. *Advances in Civil Engineering*, *2021*, 6695304. https://doi.org/10.1155/2021/6695304

[6] Guo, W., Li, H., Chen, J., & Wang, S. (2021). Numerical simulation on floor stress distribution of roadway driving along goaf in close-distance coal seams. *Shock and Vibration*, *2021*, 6615460. https://doi.org/10.1155/2021/6615460

[7] Zhang, X., Liu, H., Wang, J., & Zhao, Y. (2022). Numerical investigation of floor stress redistribution and its effect on roadway stability in close coal seam group mining. *Geotechnical and Geological Engineering*, *40*(6), 2809-2824. https://doi.org/10.1007/s10706-022-02093-7

[8] Liu, Y., Zhou, K., & Li, P. (2023). Analysis of stress evolution characteristics and floor stability in deep close-distance coal seam mining. *Sustainability*, *15*(14), 10955. https://doi.org/10.3390/su151410955

[9] Wang, J., Zhang, Z., & Feng, R. (2024). Floor stress transfer and roadway deformation law under close-distance multi-seam mining: Insights from numerical simulation and field observation. *International Journal of Mining Science and Technology*, *34*(3), 451-463. https://doi.org/10.1016/j.ijmst.2023.11.008

[10] Zhang, C., Feng, R., Zhang, X., & Shen, W. (2020). Numerical study on stress relief and fracture distribution law of floor in short-distance coal seams mining: A case study. *Geotechnical and Geological Engineering*, *38*(2), 1. https://doi.org/10.1007/s10706-019-01108-5

[11] Zhang, Z., Deng, M., Wang, X., Yu, W., Zhang, F., & Dao, V. D. (2020). Field and numerical investigations on the lower coal seam entry failure analysis under the remnant pillar. *Engineering Failure Analysis*, *115*, 104638. https://doi.org/10.1016/j.engfailanal.2020.104638

[12] Li, K., Liu, W., & Zhou, X. (2021). Investigation on surrounding rock stability control technology of high stress roadway in steeply dipping coal seam. *Advances in Civil Engineering*, *2021*, 5269716. https://doi.org/10.1155/2021/5269716

[13] Song, C., Hu, X., Chen, Z., Zhang, Y., Liu, J., & Wu, H. (2024). Study on stress–fluid coupling of coal seam floor water outburst based on FLAC3D simulation. *Chemistry and Technology of Fuels and Oils*, *59*(11), 1304-1312. https://doi.org/10.1007/s10553-024-01648-3

[14] Wang, P., Zhao, J., Feng, G., & Wang, Z. (2018). Interaction between vertical stress distribution within the goaf and surrounding rock mass in longwall panel systems. *Journal of the Southern African Institute of Mining and Metallurgy*, *118*(7), 745-752. https://doi.org/10.17159/2411-9717/2018/v118n7a4

[15] Zhou, Y., Liu, H., & Zhang, T. (2025). Theory and numerical simulation study on the plastic slip failure mechanism of multi-layered coal seam floors: A case analysis. *Frontiers in Earth Science*, *13*, 1563202. https://doi.org/10.3389/feart.2025.1563202

[16] Gao, Y., Chen, P., Zhang, X., Liu, W., & Sun, Q. (2022). Research on behavior of underground pressure in shallow coal seam with three-face goaf working face. *Frontiers in Energy Research*, *10*, 975602. https://doi.org/10.3389/fenrg.2022.975602

[17] Du, B., Liu, C., Yang, J., & Wu, F. (2020). Abutment pressure distribution pattern and size optimization of coal pillar under repeated mining: A case study. *Arabian Journal of Geosciences*, *13*(23), 1261. https://doi.org/10.1007/s12517-020-06177-0

[18] Jiang, S., Fan, G., Li, Q., Zhang, S., & Chen, L. (2021). Effect of mining parameters on surface deformation and coal pillar stability under customized shortwall mining of deep extra-thick coal seams. *Energy Reports*, *7*, 2138-2150. https://doi.org/10.1016/j.egyr.2021.04.008

[19] Zhao, J., & Li, G. (2016). Pressure-relief mining of the working face under the coal pillar in the close distance coal seams. *Geotechnical and Geological Engineering*, *34*(4), 1067-1077. https://doi.org/10.1007/s10706-016-0027-5

[20] Liu, S., Bai, J., Wang, X., Wang, G., Wu, B., Li, Y., & Zhao, J. (2021). Study on the stability of coal pillars under the disturbance of repeated mining in a double-roadway layout system. *Frontiers in Earth Science*, *9*, 754747. https://doi.org/10.3389/feart.2021.754747

[21] Vu, T.T., & Pham, DH. (2023). Influence of underground mining activities on the topographic surface, case study of Nui Beo Coal Mine (Vietnam). *Naukovyi Visnyk Natsionalnoho Hirnychoho Universytetu*, *2*, 33-039. https://doi.org/10.33271/nvngu/2023-2/033

[22] Vu, T.T., & Do, A.S. (2023). Determination of the rock mass displacement zone by numerical modeling method when exploiting the longwall at the Nui Beo Coal Mine, Vietnam. *Mining of Mineral Deposits*, *17*(1), 59-66. https://doi.org/10.33271/mining17.01.059

[23] Mu, H., Bao, Y., Song, D., Su, D., & Li, D. (2021). Investigation of strong strata behaviors in the close-distance multiseam coal pillar mining. *Shock and Vibration*, *2021*, 1263275. https://doi.org/10.1155/2021/1263275

[24] Piao, C., Lei, S., Yang, J., & Sang, L. (2019). Experimental study on the movement and evolution of overburden strata under reamer-pillar coal mining based on distributed optical fiber monitoring. *Energies*, *12*(1), 77. https://doi.org/10.3390/en12010077

[25] Shan, R., Li, Z., Wang, C., Wei, Y., Tong, X., Liu, S., & Shan, Z. (2021). Study on the distribution characteristics of stress deviator in the surrounding rock when mining closely spaced coal seams. *Environmental Earth Sciences*, *80*, 602. https://doi.org/10.1007/s12665-021-09891-1

[26] Le, P.Q., Le, H.T.T., & Nguyen, L.Q. (2024). Stress distribution under coal pillars in the case of multi-seam mining: A case study at Thong Nhat Coal Mine, Vietnam. *Journal of Hydro-Meteorology*, *20*, 15-23. https://doi.org/10.36335/VNJHM.2024(20).15-23

[27] Wang, W., Fan, C., Wang, X., Li, Z., & Wang, J. (2024). Study on the reasonable width of coal pillar based on limit equilibrium theory and numerical simulation. *Applied Sciences*, *15*(1), 314. https://doi.org/10.3390/app15010314

[28] Wang, R., Jiang, Y., Liu, J., Song, Z., & Li, J. (2021). Structure partition and reasonable width determination of coal pillar in steeply inclined extra-thick coal seams. *Lithosphere*, *2021*(1), 6059167. https://doi.org/10.2113/2021/6059167

[29] Xing-Zhi, Z. (2011). Stability analysis of roadway surrounding rock based on limit equilibrium theory. *Procedia Engineering*, *26*, 2380-2386. https://doi.org/10.1016/j.proeng.2011.11.2410

[30] Babets, D., Sdvyzhkova, O., Shashenko, O., Kravchenko, K., & Cabana, E.C. (2019). Implementation of probabilistic approach to rock mass strength estimation while excavating through fault zones. *Mining of Mineral Deposits*, *13*(4), 72-83. https://doi.org/10.33271/mining13.04.072

[31] Le, T.D., & Oh, J. (2022). Longwall face stability analysis from a discontinuum-discrete fracture network modelling. *Tunnelling and Underground Space Technology*, *124*, 104480. https://doi.org/10.1016/j.tust.2022.104480

[32] Li, G., Wang, H., Zhang, Y., & Liu, X. (2025). Optimization of small coal pillar width and control of surrounding rock stability under close-distance coal seam mining. *Scientific Reports*, *14*, 74793. https://doi.org/10.1038/s41598-024-74793-8

[33] Itasca Consulting Group, Inc. (2019). *Fast Lagrangian analysis of continua (FLAC3D) user's guide (Version 6.0)*. Minneapolis, United States: Itasca. Retrived from: https://www.itascacg.com/search

Чисельне моделювання розподілу напружень в підошві під вугільними ціликами та стійкість виробок у близькорозташованих вугільних пластах

К.Ф. Ле, Т.Т. Ву

Мета. Дослідження закономірностей розподілу напружень під вугільним ціликом верхнього пласта для визначення раціонального розташування підготовчої виробки в нижньому пласті в умовах близького залягання пластів вугільної шахти Тхонг Нят (В'єтнам) із застосуванням методів сучасного чисельного моделювання.

Методика. Для вивчення розподілу та перерозподілу напружень під вугільним ціликом і виробленим простором побудовано чисельну модель у програмному середовищі FLAC3D. Ураховано вертикальні та горизонтальні компоненти напружень, фізико-механічні властивості порід і реальні граничні умови.

Результати. Розглянуто для порівняння чотири варіанти розташування виробки: під центром цілика (A), під його краями (B, C) та у підошві під виробленим простором (D). Чисельні розрахунки показали, що максимальна концентрація напружень спостерігається у варіанті A – коефіцієнт концентрації становить 2.4-2.7 від початкових напружень, що створює високий ризик втрати стійкості. Варіанти B і C характеризуються меншими, але все ще значними напруженнями, обумовленими навантаженням від цілика. Натомість варіант D демонструє істотно нижчий і рівномірніший розподіл напружень та меншу зону розвитку пластичних деформацій, що є

сприятливим для збереження стійкості виробки. Доведено, що вибір місця розташування виробки є вирішальним чинником безпеки та довговічності гірничого об'єкта.

Наукова новизна. Встановлено, що найбільш раціональним і безпечним є розташування виробки у підошві під виробленим простором поза межами вугільного цілика, на горизонтальній відстані близько 5 м (варіант D) Для геологічних умов шахти Тхонг Нят, при цьому слід уникати проходження виробки безпосередньо під ціликом.

Практична значимість. Отримані результати формують наукове й практичне підґрунтя для проєктних рішень, підвищення стійкості виробок, зниження витрат на їх утримання та забезпечення безпечних умов праці у шахтах із близькорозташованими пластами.

Ключові слова: *вугільний цілик, вугільні пласти, розподіл напружень у підошві, гірський тиск, стійкість виробки, шахта Тхонг Нят*

Publisher's note

All claims expressed in this manuscript are solely those of the authors and do not necessarily represent those of their affiliated organizations, or those of the publisher, the editors and the reviewers.